AD-A137 518 EFFECTS OF FATIGUE ON THE G P ZONES IN AL-ZN ALLOYS(U) 1/1
NORTHWESTERN UNIV EVANSTON IL DEPT OF MATERIALS SCIENCE
R G PAHL ET AL. 16 JAN 84 TR-13 N00014-80-C-0116
UNCLASSIFIED F/G 11/6 NL

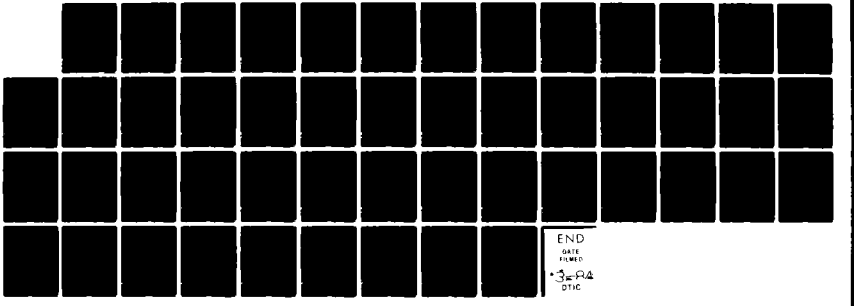

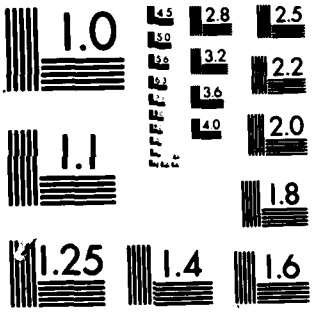

(1)

NORTHWESTERN UNIVERSITY

DEPARTMENT OF MATERIALS SCIENCE

Technical Report No. 13
January 16, 1984

Office of Naval Research
Contract N00014-80-C-116

EFFECTS OF FATIGUE ON THE G. P. ZONES IN Aℓ-Zn ALLOYS

by

R. G. Pahl, Jr. and J. B. Cohen

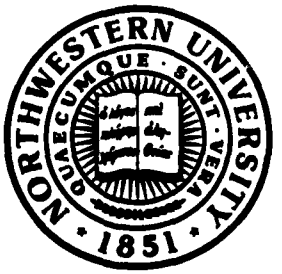

EVANSTON, ILLINOIS

EFFECTS OF FATIGUE ON THE G.P. ZONES IN AL-ZN ALLOYS

R.G. Pahl,Jr. and J.B. Cohen

ABSTRACT

Small-angle X-ray scattering has been employed to study the stability of G.P. zones in two Al-Zn alloys during fatigue, in order to provide statistically sound information on this process. In a 5.3 at. pct. Zn alloy containing $\sim 10^{25}$ zones per m^3 with an average diameter of 18 A, the normally sluggish coarsening was accellerated by fatigue at room temperature by factors of 10^6-10^7 except near a fatigue crack. Reverted samples aged rapidly during fatigue at room temperature, but in a reverted sample of Al-3.5 at. pct. Zn cycled at 77°K no appreciable zone growth occurred. Upon warming this sample to room temperature (without any load) rapid clustering took place. These results imply that a vacancy fraction of 10^{-5}-10^{-6} was produced by the fatigue, and this excess vacancy concentration appears to be the cause of the zone growth during cycling at room temperature.

R.G.PAHL,Jr.,formerly research assistant, Department of Materials Science and Engineering, The Technological Institute, Northwestern University, Evanston IL, 60201 is now with Argonne National Laboratory, Idaho Falls, Idaho,83401. J. B. COHEN,Fellow AIME and ASM, is the Frank C. Engelhart Professor of Materials Science and Engineering and Technological Institute Professor, Northwestern University.

INTRODUCTION

Precipitation-hardened alloys are known to be particularly vulnerable to the plastic strain localization which accompanies fatigue. Most theoretical attempts at explaining the poor fatigue resistance of these materials are based on the evolution, stability, and redistribution of the precipitate structure during fatigue. Mechanisms based on particle disordering[1], overaging[2], reversion[3], Ostwald ripening[4], and aging inhomogeneities[5] have been suggested. These conflicting interpretations have been based primarily on evidence obtained with the transmission electron moicroscope, by imaging the local fatigue-induced structure within persistent slip bands (psb's). Precipitate-dislocation interactions can easily be obscured in such regions of high deformation. Also, the sample volume which can be examined is necessarily small, and may not be representative of the overall response. Destructive sample preparation techniques often prevent convincing "before and after" images throughout the various stages of fatigue.

Small-angle X-ray scattering (SAXS) has been used in this investigation to obtain for the first time a quantitative estimate of the changes in G.P.zones in Al-Zn alloys due to fatigue. Bulk samples of Al-3.5 and 5.3 at. pct. Zn have been cycled to

failure in fully reversed loading at both room temperature and 77 ^{o}K. The initial heat treatments have been varied to permit characterization of the damage at various stages of the age- hardening process. At the same time as this study[6] Steiner et al[7] reported some preliminary results on Cu-Co alloys, employing small-angle neutron scattering.They suggested that reversion occurred, primarily in the psb's, but unfortunately they examined only two specimens and in only one of these did the changes exceed experimental error.(They reported decreases in the volume fraction of zones, but this requires extrapolation of the data in a region where the form of the scattering is not exactly known and the extrapolated portion is a significant contribution to the result.)

EXPERIMENTAL PROCEDURES

Specimens

Dog-bone shaped fatigue samples were spark cut from alloy sheet which had been strain annealed to coarsen the grain size to 1-3 mm. The specimen design was based on the need to facilitate the measurements of small-angle X-ray scattering. The coarse grain size was large enough to contain the 0.35mm X-ray beam, and the specimen was made thin enough to allow penetration of this beam. The nominal dimensions are shown in Fig.1. The heat treatments given to the six specimens are summarized in Table I.

Fatigue Testing

Tension-compression cycling was carried out in laboratory air at room temperature and in dynamic displacement control (unless otherwise noted). An Instron model 1251 electrohydraulic fatigue machine was employed. Low temperature tests were carried out on a specially designed apparatus[8]. The sample was cycled in load control within a Dewar flask containing liquid nitrogen. In all tests, an anti-buckling jig was attached to the specimen[9,10]. Because each sample was thin enough to pass the X-ray beam, buckling could occur at small compressive loads, and lateral displacement was restricted with flat Al plates clamped around lubricated Teflon gaskets. The cycling frequency at room temperature was usually 0.1 Hz, but this was increased to 5 Hz for high-cycle fatigue. The low temperature testing was run at .023 Hz, to assure smooth operation of the anti-buckling jig in the liquid nitrogen bath.

A sketch of a hysteresis loop is given in Fig.2, to illustrate the nomenclature to be followed in this paper. The plastic strain, $\Delta\varepsilon_{PL}$, was obtained from the loop width at zero load. The peak stress, σ_{max}, is the average for the tensile and compressive halves of the loop.

Small-Angle Scattering

The X-ray measurements were obtained with a Rigaku-Denki model 200PL 12 kw rotating anode generator. A Mo target was operated with a 0.5 mm square focus at 50kV, 180 mA.(Mo radiation was chosen so that a relatively thick specimen could be used.) Pinhole collimation (0.5 and 0.3 mm slits separated by 250 mm) were employed with a Rigaku-Denki small-angle scattering goniometer. The sample was 100 mm from the second slit and a scatter slit, and the beam's path was evacuated to 10 μm. The detection system consisted of a one dimensional gas-flow proportional counter,covered with a Zr foil to emphasize the K_α radiation, and 324 mm from the sample. This detector was interfaced through a multi-channel analyzer to a DEC PDP8/E minicomputer[11]. The system's linearity was examined by displacing the detector known amounts in front of a narrow X-ray beam. The detector resolution was ~ 0.05° 2θ. The intensity of a peak from a film of polyethylene in the beam was sometimes employed to normalize different measurements with a given sample. However, when the scattering was weak, this film was removed, because it produced some background scattering.

A sample could be positioned in the X-ray beam in a reproducible fashion, so that the same area in any grain could be exam-

ined at each step of any sequence of cycling. This was accomplished by painting a small dot of X-ray sensitive phophor on the spot to be examined. With the room lights dimmed, the sample could be placed so as to maximize the phosphor's brightness in the X-ray beam. Once the specimen was in the desired position, the phosphor was rinsed away with methyl alcohol. By tilting a specimen around an axis parallel to the X-ray beam, any anisotropy in the scattering could be detected. The data were analyzed with computer code for the miniprocessor, applying the theory of small-angle scattering summarized in the Appendix.The quantities determined were: 1) the Guinier radius, R_{GLS} ,where the subscripts LS imply a least squares solution to the intensity (this radius is a measure of the moment$\langle R^8\rangle/\langle R^6\rangle$), 2)the Porod radius, R_{PLS} ($\langle R^3\rangle/\langle R^2\rangle$), 3)the size distribution, 4)these two radii from the size distribution (indicated by subscripts SD), which by comparison with the radii from the data itself indicates the validity of the procedures employed to obtain the distribution), 5)the average diameter,$\langle D\rangle$, from the distribution, 6)the total number of zones per unit volume, N_V ,6)the integrated small-angle scattering, Q, which is a measure of the volume fraction of zones, and 7)whether or not the Porod region indicated a sharp matrix-zone interface. All measurements at room temperature were made immediately following fatigue, to minimize recovery. For the test at 77° K, a special cryogenic sample stage was added to

the SAXS goniometer, which maintained the sample at 178° K. This consisted of a large copper rod extending from within a liquid nitrogen bath, and to which the sample was clamped.. A plexiglass clinder around this rod was purged continuously with cold, dry nitrogen gas. Thin Mylar windows for the X-ray beam were cemented to this cylinder, and a fan blowing cold air was directed at the frame to prevent condensation of moisture. The transfer of the sample from the nitrogen bath on the fatigue machine to this device was made under liquid nitrogen.

RESULTS

Aged Al-5.3 at. pct Zn

a)Spherical G.P. Zones, 18 Å in Average Diameter

Sample V (see Table II) was cycled to failure in total displacement control, with a total plastic strain, ~3.5 pct. (For all specimens, hysterisis loops and microphotographs of the surface can be found in ref. 6.) Faint slip lines were observed on the surface of the sample at failure.An uncracked grain was chosen for the pre-fatigue and post-fatigue comparisons. (The dominant failure mode in these alloys is grain boundary separation, which is most likely due to the precipitate -free zone bordering these boundaries [12].) The parameters determined from the

small-angle X-ray scattering are summarized in Table III and Fig.3.

Comparison of the SAXS parameters before and after fatigue reveals that fatigue reduced the number of small zones, while increasing the number of large ones. This is evident from the steeper slope of the Guinier plot in Fig.3 after fatigue than before, and as well, the shift in the size distribution to larger sizes. Fatigue did not alter the amount of solute in the matrix, because the integrated intensity (Q in Table III) was constant; this value is directly related to the solute in the zones and hence their volume fraction, since the zone composition is fixed.

The increase in average zone diameter by 35 pct., the constant volume fraction, and the reduction in the total number of zones by 60 pct suggests that Ostwald ripening took place during cycling. Coarsening at this stage of aging is normally sluggish in the absence of deformation, and so it is remarkable how much zone growth occurred in the 25 minutes it took for the fatigue test.

b)Spherical G.P. Zones, 24 Å in Average Diameter

Sample T was examined in two stages of fatigue, described in

Table II. Two separate locations on the sample were examined with SAXS.The region examined before fatigue, and after two sets of cycles, was located within an uncracked grain showing faint slip markings. The other grain (examined only after the second number of cycles) contained one of the few transgranular deformation markings in the gage section, and which appeared to be associated with the linking of grain boundary cracks. The SAXS results are summarized in Table III. Essentially no change in the size or amount of the zones occurred in the uncracked grain.(It is interesting to note that this is the same result reported in ref.7 for Cu-Co alloys with about the same zone size or larger.) The other grain, however, underwent a remarkable change in scattering power, as can be seen in Fig.4. Tilting the sample about an axis parallel to the incident X-ray beam revealed the anisotropic nature of the scattering pattern. This anisotropy indicated oriented plate- like zones. It is well known that that there are intermediate phases (R and α') which are platelike in form[13]. Following refs. 14 and 15, the scattering patterns were analyzed in terms of platelets of thickness t, diameter D, and volume V, and the resultant values are given in Table III.

Consideration of all the data on sample T in this table indicates that a sample fully aged to contain large spherical G.P. zones experienced negligible solute redistribution within un-

cracked grains at low cyclic plastic strain. However, in the deformation front associated with an advancing crack , coarsening was accellerated. Assuming no appreciable change occurred in the solute content of the matrix, approximately twenty spherical zones were destroyed (dissclved) for each large platelet that formed.

c) Ellipsoidal G.P. Zones

Specimen R was aged to form ellipsoidal zones, and was cycled in fully reversed loading under plastic strain control. The fatigue parameters are summarized in Table II. Prior to fatigue, the scattering showed a variation in R_{GLS} of ~ 20 pct with tilt of the specimen around the incident X-ray beam, which indicates that the ellipsoidal zones had a preferred orientation in the grain examined. The results after fatigue are in Table III. There was essentially no change in the size or amount of the zones in the (uncracked) grain that was examined. This could be due to the low driving force for coarsening at this late stage of aging, or a dynamic balance between a reduction in size (by cutting of the zones by dislocations) and coarsening.

Underaged 3.5 and 5.3 at. pct. Zn

The reversion theory of fatigue softening[3] suggests that G.P. zone dissolution occurrs by shearing within persistent slip bands. The remaining fragments of G.P.zones would be subcritical in size and dissolve, leaving a band of supersaturated solid solution in the interior of a psb. Strain would become increasingly localized, and cracks could initiate easily in these weaker regions. The fatigue-induced overaging reported in the previous section suggests that in the case of alloys aged extensively, any solute resulting from reversion does not remain in the matrix, but instead re-precipitates on nearby large zones or platelike precipitates. In order to characterize the effects of fatigue on a supersaturated solid solution, three samples were cycled in the underaged condition. Samples S (5.3 at. pct. Zn) and P (3.5 at. pct. Zn) were given the thermomechanical treatments described in Table I. The procedures indicated were chosen to strengthen the precipitate-free zones adjacent to grain boundaries, by introducing a stable tangle of dislocations in these regions, and then reforming the zones more homogeneously, following ref 16. A modest improvement in high-cycle lifetime was reported in this reference. A third sample,L(3.5 at. pct. Zn) was cycled in liquid nitrogen in the reverted condition.

a) Sample S

As shown in Fig. 5, the reaging of this sample produced little change in the SAXS pattern, compared to the reverted state. It was then cycled (with dynamic displacement control) in three stages. The first consisted of 15 cycles over which the total strain level was raised to 0.35 pct., and then 20 cycles were applied. Following measurements of the SAXS, a second set of cycles was carried out in total plastic strain control ($\Delta\varepsilon_{PL}$ =0.1 pct.) followed by measurement of the SAXS. The final cycling ended in failure after 10 additional cycles at the same strain level.

Surface slip striations were much deeper and more closely spaced than those on the fully aged specimens. An intergranular crack and severe slip activity were observed in grains adjacent to the one examined with X-rays. The scattering curves are given in Fig.5 for each stage. A remarkable increase in this scattering due to fatigue is evident. The various parameters from these curves are summarized in Table III, where it can be noted that there was a dramatic increase of the total intensity over that for the solid solution; this can also be seen in Fig.5. Also, the results in the table indicate that nucleation and growth of G.P.zones occurred during fatigue. In only 20 minutes of room-temperature fatigue the total volume fraction of zones that could form did so. In addition to the nucleation of new zones,

there was a decrease in the number of large zones (those greater than ~40 Å in diameter). Thus, some dissolution did occurr as part of the process, as well as coarsening.

b) Sample P

While this sample of 3.5 at. pct. Zn underwent the same TMT treatment as the more concentrated alloy (sample S), the re-aging step produced no detectable precipitation in this more dilute alloy. Sample S was never exposed to the high-cycle regime, so the testing of sample P was begun at low aplied strains. Cycling (in displacement control) was broken into nine separate sets, each of which was followed by examination of the SAXS. The fatigue parameters are given in Table II. the first six sets were in the elastic regime, while in the last three sets, gradually increasing levels of total strain were applied.

Fig. 6 shows the dramatic increase in scattering power due to fatigue after plastic strain cycling began (set 7). The weakest scattering pattern in this figure corresponds to that registered after the cycles for set 4, and is the same as the pattern for the as-reverted state. After the cycles in set 6 the pattern is approximately twice this level, and is due to only slight clustering, that is the formation of solute pairs and triplets.

The parameters evaluated from these curves (for the last three sets) are summarized in Table III. Nucleation and growth of zones occurred up to the end of set 8, and during set 9 only Ostwald ripening took place; the number of zones decreased while the size increased at constant volume fraction of zones.

Thus, small "polymers", involving only a few Zn atoms, form in a supersaturated solid solution when it is cycled near the elastic limit. Fatigue of this lightly clustered state well into the plastic regime rapidly increases the nucleation and growth rates of G.P. zones.

c) Fatigue at 77 K, Sample L

Sample L (3.5 at. pct. Zn) was solution heat-treated and quenched in the same manner as sample P (also 3.5 at. pct Zn). However, no TMT treatment was applied, and following reversion, no artificial aging treatment was employed. Because re-aging at room temperature following reversion is slow in dilute Al-Zn alloys, sample L was cycled in an essentially homogeneous condition, in stress control at 100 MPa for 100 cycles at 77° K. (No cracks were observed after the tests.) The first SAXS patterns were recorded immediately after fatigue with the sample at 178°K. At no time during or after fatigue did the sample temperature

ever exceed this value. After X-ray patterns were taken, the sample was warmed to room temperature and SAXS was obtained from two different grains.

The scattering patterns after fatigue (taken at 178° K)are shown in Fig.7a. the weakest curve was collected with the X-ray beam located in the undeformed grip section, and illustrates the diffuse scattering typical of the as-reverted state. The size distributions are shown in Fig. 7b, and the various parameters obtained from the data are included in Table III.

Solute diffusion at 77° K is negligible and therefore the pattern taken at 178°K represents the (small) amount of clustering that occurred at this latter temperature during the time it took to obtain the data (~12 hrs). Employing estimates of the zone composition at this temperature[17],it can be shown that the integrated SAXS implies that the solute content of the matrix was the equilibrium value; that is, all the solute that could be in zones was in such regions at this point. The patterns from the two grains that were subsequently examined at room temperature indicate that the fatigue-enhanced aging varied from grain to grain, probably depending on the local value of the critical resolved shear stress. These two patterns show clearly that zone growth occurred upon warming the sample to room temperature.

Since zone growth took place at both 178°K and 298°K without any load being applied, it can be inferred that vacancies in large quantities were produced by fatigue at 77°K, and were retained in the alloy. A dynamic dislocation mechanism for solute redistribution during fatigue is not required.

DISCUSSION

While it is well known that fatigue produces vacancies[18], this is the first report to show directly that the concentration is so large that it can produce rapid nucleation, growth, and coarsening. This was first suggested by Broom et al[19] based on mechanical behavior. It is difficult to calculate this excess vacancy concentration from first principles because of the variety of dislocation configurations and interactions that develop during cycling. An empirical estimate, due to Seitz[20] is based on a linear relationship between vacancy content and applied strain:

$$N_V \cong 10^{-4} \epsilon_{PL}, \qquad (1)$$

where N_V is the fraction of vacant lattice sites. Another estimate is possible by comparing the coarsening rates observed in this study with that predicted by the theory of Ostwald ripening. Greenwood[21] has derived a convenient expression for this process:

$$R^3_{final} - R^3_{initial} = 3 \tilde{D} C_\infty [2\gamma V_a / kT] t \ . \qquad (2)$$

Here, γ, the interfacial energy per unit surface area can be estimated for the Al-Zn system as 46×10^7 joules per m^3, from the work by Bohm and Gerold[22]. The term V_a is the volume per atom, and C_∞ the Zn concentration in a large particle can be taken from the known metastable phase diagram. The average sizes are accessible from the size distributions presented in the previous section, and the time from the known cycle frequency and the number of cycles. In this way $\tilde{D}$, the interdiffusivity, can be estimated. It is well known that $\tilde{D} \alpha N_V$. From the data of Hilliard et al[23], the equilibrium value of $\tilde{D}$ can be obtained by extrapolation, and N_V from:

$$N_V = \exp[S_f/kT]\exp[-E_f/kT] \quad , \tag{3}$$

where S_f and E_f are the entropy and energy for vacancy formation (taken from Horak et al[24]). By obtaining $\tilde{D}$ during fatigue from Eq.2 and the ratio $\tilde{D}/N_V$ from Hilliard's data and Eq.3, N_V can be obtained. The results of these calculations are given in Table IV. Diffusivities and vacancy concentrations are enhanced by fatigue by 10^6 -10^7. [The values for sample S, and the early sequence for P are underestimated, because a constant volume fraction of zones was not present, and nucleation occurred, as well. Also, for sample L, the time at room temperature without load was employed. For those samples cycled at increasing strain, only those cycles beyond the elastic limit were counted in making

these estimates.]

The remarkable agreement between Seitz' estimate (Eq.1) and the values in Table IV is shown in Table V.

The rapid coarsening of sample L at 178° K results in the physically unreasonable vacancy concentration of 1.6 pct. Ceresara and Federighi[25] have suggested that divacancies cause diffusion at this temperature, so that it is inappropriate to extrapolate the diffusivity in ref.23 from high temperature in this case.

CONCLUSIONS

1) Small-angle X-ray scattering has proven to be a powerful technique for characterizing the effects of fatigue on G.P. zones.

2) Samples aged to contain an equilibrium volume fraction of small, densely spaced spherical G.P. zones coarsen at rates exceeding the theoretical equilibrium value by approximately six orders of magnitude at room temperature.

3) Samples fully aged to contain large widely spaced spherical or ellipsoidal zones resist coarsening, either because of the small driving force late in the aging process, or because of a dynamic balance between cutting processes and ripening.

4) Even in this second case, in areas of a sample adjacent to the

crack path, zones undergo accellerated transformation.

5) Nucleation, growth, and coarsening can occur in very short times during cycling of a supersaturated solid solution produced by reversion, even when normal aging in such a condition is sluggish. TMT including such cycling could be a useful step in processing.

6) Vacancies generated by high-stress cycling at 77 K are immobile at this temperature, but promote rapid aging above 178 K in Al-Zn alloys.

ACKNOWLEDGEMENTS

This research, supported by ONR under contract no.N00014-80-C-0116, was submitted (by R.G.P.) in partial fulfillment of the requirements for the Ph.D. degree at Northwestern University in May 1983. The diffraction, fatigue, and mechanical properties facilities of Northwestern University's Materials Research Center were employed; these laboratories are supported in part by NSF under grant No.DMR-MRL-82-16972. Dr. M. Yang helped with the software, and Prof. T. Gross made valuable suggestions concerning fatigue testing. Discussions with Prof. M.E. Fine are gratefully acknowledged.

APPENDIX

For a spherically symmetric particle the scattered intensity can be expressed as[15]:

$$I(h) = I_e(h)\langle F^2(h)\rangle = I_e(h)\left[\int_0^\infty \rho(r)[\sin hr/hr]4\pi r^2 dr\right]^2 , \qquad (A1)$$

where $I_e(h)$ is the intensity scattered by one electron, $\rho(r)$ is the electron density, r is measured from the particle center and $h=4\pi\sin\theta/\lambda$. For small scattering vectors, the Guinier approximation descibes the scattering from randomly oriented spherical particles:

$$I(h) = I(o)\exp[-h^2R_g^2/3], \qquad (A2)$$

where R_G is the radius of gyration. For a single particle of radius R_S, $R_G=(3/5)^{\frac{1}{2}}R_S$. The radius of gyration in the presence of a size distribution is:

$$R_G = [(3/5)\langle R^8\rangle/\langle R^6\rangle]^{\frac{1}{2}} . \qquad (A3)$$

At large h, the Porod approximation for Eq.1 is:

$$I(h) \cong 2\pi^2\Delta\rho^2 I_e(h)S_{TOT}h^{-4}, \qquad (A4)$$

where S_{TOT} is the total external surface area of the scattering particles under the X-ray beam. (In this case it is assumed that

the particles have sharp interfaces.) Thus, a plot of $h^4I(h)$ vs. h approaches a value directly proportional to surface area.

The integral small-angle scattering (for point collimation) is:

$$Q = \int_0^\infty h^2 I(h)dh, \tag{A5}$$

and can be shown to be related to the solute concentration inside and outside a particle in a binary system[26]:

$$(\tfrac{1}{2}\pi)^2 \int_0^\infty h^2 I(h)dh \cong (m_1 - \langle m \rangle)(\langle m \rangle - m_2)(\Delta Z^2/V_a). \tag{A6}$$

The overall solute concentration is <m>, the paricles have concentration m_1, and the matrix, m_2. The term ΔZ is the difference in atomic number of the two elements, of average volume V_a. Alternatively[15],

$$Q = 2\pi^2 I_e(h)\Delta\rho^2 V_S C(1-C), \tag{A7}$$

where $\Delta\rho$ is the electron density difference between particle and matrix, V_S is sample volume, and C is volume fraction(of particles). If the absolute intensity can be measured from two alloys at any given temperature, Eq. A6 can be employed to determine m_1 and m_2 [27], and hence the metastable miscibility gap; this has been done in the Al-Zn system[27]. Absolute scattering power was not determined in this investigation, and a ratio technique was

employed to determine the volume fraction of G.P.zones[28]. Assuming that does not change with fatigue, increases in the relative value of Q correspond to increases in the volume fraction precipitated, according to Eq. A-7. It is known that full aging occurs rapidly in dilute Al-Zn alloys quenched directly from the α phase and therefore the ratio of the Q value after fatigue to that prior to fatigue gives the actual volume fraction (after cycling).[28].

Another moment of the size distribution is the Porod radius:

$$R_p = \langle R^3 \rangle / \langle R^2 \rangle = [3\int_0^\infty h^2 I(h)dh]/(1-C)\lim_{h\to\infty} h^4 I(h) \qquad (A8)$$

Particle diameter distributions were obtained by using the integral transform derived by Letcher and Schmidt[29]. They have shown that the relative diameter distribution function, N(D), is given by:

$$N(D)\alpha D^{-2}\int_0^\infty [h^4 I(h) - C_4]\alpha(hD)dh, \qquad (A9)$$

where D is the particle diameter, C_4 is the limit $h^4 I(h)$ ($h \to \infty$), and $\alpha(hD)$ is the single particle form factor, given (with x=hD) as:

$$\alpha(X) = (1-8/X^2)\cos X - (4-8/X^2)(\sin X/X) .$$

The value of C_4 is obtained following ref. 30 to assure that the integral in Eq. A9 converges.

The data collected in this research were corrected for sample absorption, counting time differences, sample volume, and parasitic scattering. The last contribution (from slits, windows,etc.) was determined by making a measurement witout a sample in place. This intensity was small beyond the beam stop at 0.15 2 .

REFERENCES

1.C. Laird,V.J. Langelo,M. Hollrah,N.C. Lang,and R.de la Veaux:Mat. Sci. Eng.,1978,vol.32,p.137.

2.J. B. Clark and A.J. McEvily:Acta metall.,1964,vol.12,p.1359.

3.W. Vogel,M. Wilhelm,and V. Gerold:Acta metall.,1982,vol.30,p.21.

4.S. Brett and R.D. Doherty:Mater. Sci. Eng.,1968,vol.32,p.255.

5.C. Laird and G. Thomas:Int. J. Fract. Mech.,vol.3,p.81.

6.R.G. Pahl,Jr.:Ph.D. thesis,Northwestern University,August,1983.

7.D. Steiner,R. Beddoe,V. Gerold,G. Kostorz, and R. Schmelczer:Scripta metall., 1983,vol.17,p.733.

8.P.K. Liaw and J. Baker:Rev. Sci. Instrum.,1979,vol. 50,p.1590.

9.W. Ramberg and J.A. Miller:J. Aeronautical Sci.,1946,p.569.

10.M. Kiritani and S. Weissman:Metall. Trans.,1972,vol.3,p.1229.

11.M.R. James,Ph.D. thesis, Northwestern University,January,1977.

12.G.W. Lorimer and R.B. Nicholson:The Mechanism of Phase Transformations in Crystalline Solids, Institute of Metals, London,1969.

13.P. Bartuska and M. Simerska:Czech. J. Phys.B,1978,vol.28,p.1047.

14.O.A. Pringle and P.W. Schmidt:J. Colloid and Interface Sci.,1977,vol.60, p.252.

15.A. Guinier and G. Fournet:Small-Angle Scattering of X-rays,Wiley,New York, 1955.

16.M.C. Lu and S. Weissman:Mater. Sci. Eng.,1977,vol.32,p.41.

17.K.G. Satyanarayana:J. Mat. Sci.,1981,vol.16,p.1233.

18.R.L. Segall and P.G. Partridge:Phil. Mag.,1959,vol.4,p.912.

19.T. Broom, J.H. Molineux, and V.N. Whittaker:J. Inst. Met.,1956,vol.84,p.356.

20.F. Seitz:Adv. in Phys.,1952,vol.6,p.43.

21.G.W. Greenwood:Acta metall.,1956,vol.4,p.243.

22.G. Bohm and V. Gerold:Scripta metall.,1970,vol.4,p.269.

23.J.E. Hilliard,B.L. Averbach,and M. Cohen:Acta metall.,1959,vol.7,p.86.

24.J.A. Horak,T.H. Blewitt,and M.E. Fine:J. Appl. Phys.,1968,vol.39,p.326.

25.S. Ceresara and T. Federighi:Phil. Mag.,1968,vol.18,p.301.

26.V. Gerold and W. Merz:Scripta metall.,1967,vol.1,p.33.

27.V. Gerold:Phys. Stat. Sol.,1961,vol.1,p.37.

28.S.D. Harkness and R.W. Gould:Adv. in X-ray Analysis,1969,vol.12,p.97.

29.J.H. Letcher andP.W. Schmidt:J. Appl.

Phys.,1966,vol.37,p.649.

30.O.L. Brill and P.W. Schmidt:J. Appl. Phys.,1968,vol.39,p.2274.

TABLE I

HEAT TREATMENTS

Sample ID	Nominal Composition a/o Zn	Solution Treatment*	Preaging Treatment***	Aging Treatment	Prefatigue State
V	5.3	698°K/14 hrs.	523°K/30 min.	Room Temp./5.5 mos	Small GP zones
T	5.3	698°K/14 hrs.	523°K/30 min.	Room Temp./6 mos.	Large GP zones
R	5.3	698°K/14 hrs.	523°K/30 min.	Room Temp./7.3 mos.	Ellipsoidal GP zones
S	5.3	698°K/14 hrs.**	423°K/20 min.	373°K/18 hrs.****	GP zones (underaged)
P	3.5	698°K/14 hrs.**	423°K/20 min.	351°K/64 hrs.****	~ homogeneous
L	3.5	698°K/14 hrs.**	423°K/20 min.	Room temp./14 days	~ homogeneous

* All samples air cooled from solution T.

** Prior to further treatment, an additional 1 hr/698°K followed by a H_2O quench. For samples S and P, this preceded 2×10^4 cycles at ± 22.8 MPa.

*** Drop quenched in 298°K H_2O bath after preaging treatment.

****Aged in stirred oil bath.

TABLE II

Fatigue Response of Samples

Sample	N (cycles)	$\Delta\epsilon_{PL\,TOT}$ (%)	$\Delta\epsilon_{PL}$ (%)	σ_{max} (MPa)
V°	1		.16	210.3
	2		.15	213.1
	10		.10	221.1
	20		.10	223.4
	50		cracking apparent	
	130		test stopped, SAXS	
T°	1		.028	173.8
	2		.026	173.8
	5		.018	180.0
	10		.013	179.3
	20		.014	180.6
	50		.013	180.0
	100		.015	180.0
			-SAXS	
	101		.014	177.2
	115		.014	176.5
	150		.013	175.1
	200		.013	175.1
	250		.014	174.4
	300		.015	171.7
	350		cracking evident	168.2
	380		test stopped, SAXS	
R+	1	.72	.14	206.8
	2	.72	.13	209.6
			-SAXS	
	3	.72	.13	219.2
	4	.72	.11	224.1
	5	.75	.14	228.2
	10	.75	.11	239.2
	12	.80	.15	245.4
	20	.83	.12	247.5
	21	.83	.15	247.5
	30	crack ng evident - test stopped, SAXS		
S	2	N refers .05	---	17.9
	2	to num- .10	---	35.8
	2	ber of .15	.016	45.7
	2	cycles at .20	.052	51.7
	2	each strain .25	.082	58.3
	1	↓ .30	.110	66.3
	4	N refers .30	.088	76.3
	1	to Nth .35	.120	85.5
	7	cycle at .35	.092	90.5
	9	that .35	.079	94.8
	20	strain .35	.044	106.9

			-SAXS	
	21	N refers	.35	.020	115.8
	26	to total	.40	.053	122.7
	28	number of	.45	.088	125.5
	30	cycles	.48	.095	130.3
	32		.50	.108	138.6
	42		.60	.160	153.7
	44		.55	.105	155.8
	45		.55	.095	162.7
	65		.55	.070	165.5
	68	(N refers	.60	.110	171
	80	to the	.60	.090	175.1
	81	Nth cycle	.63	.102	182
	100	at given strain.)	.63	.085	184.8
				-SAXS	
	101		.50	.025	163.4
	106		.60	.085	177.2
	108		.63	.103	169.6
	110	cracking evident - test stopped, SAXS			
p^o (5Hz)	1				19.5
	500				20.2
	1,000				20.6
	1,001				19.0
	3,000				19.2
	10,000			-SAXS	19.2
	20,000				19.4
	20,003				19.0
	30,000				19.4
	40,000				19.6
	60,000				19.6
	80,000			-SAXS	19.6
	100,000				19.7
	101,000				19.0
	120,000				19.2
	150,000				19.3
	200,000				19.4
	1			-SAXS	29.8
	500				30.5
	2,000				30.8
	3,000				30.9
	4,000				31.0
	5,000			-SAXS	31.1
	5,010				29.1
	10,000				30.5
	20,000				30.6
	30,000				30.7
	40,000				30.9

o = total displacement control
+ = total plastic strain control

TABLE III

Summary of Small Angle Scattering Results

Sample V	Grain ID	$\sum_n \Delta\varepsilon_{PL}$ (%)	R_{GLS} (Å)	R_{GSD} (Å)	Flat Porod Region	R_{PLS} (Å)	R_{PSD} (Å)	[2] $\langle D \rangle_{SD}$ (Å)	N_{TOT} (m^{-3})	[3] Q	[4] $\sqrt{I/I}$
	1	Prefatigue	13.5(± .9%)	13.4	No	10.3	12.9	17.5	9.7×10^{24}	5.4	.75,2.2
	1	3.50	19.9(± 1.2%)	18.9	"	14.0	17.8	23.9	3.8×10^{24}	5.0	.71,3.2
	2	3.50	22.5(± .5%)	22.3	"	17.7	19.5	25.4	3.0×10^{24}	4.7	.46,2.7
[5] R		Prefatigue	29.2(± .91%)	----		21.1	----	----	----	4.3	.29,2.5
		.28	28.3(± .88%)	----		20.2	----	----	----	4.3	.40,4.2
		4.0	28.9(± .14%)	----		20.3	----	----	----	4.3	.29,2.5
S		Prefatigue	17.7(± 6.1%)	12.4	Yes	17.7	16.7	22.5	$.18\times10^{24}$	[10] .13	[9] 2.4, 9.1
		1.85	[6] 15.2(±5.0%)	13.6		15.2	14.5	19.5	1.4×10^{24}	1.0	1.8, 5.3
		8.60	[7] 17.6(±1.9%)	13.7	Yes	18.0	16.7	22.7	2.6×10^{24}	3.1	1.1, 5.3
		9.10	[8] 13.6(±2.8%)	9.7	No	13.6	12.9	17.5	96.8×10^{24}	5.0	1.3, 6.7
[11] P		.50%	6.0(±11.1%)	5.3	Yes	6.5	6.3	9.1	2.4×10^{25}	1.8	2.3, 5.0
		7.0%	9.0(±10.5%)	6.3		8.6	8.3	11.2	1.7×10^{25}	2.8	2.0, 5.3
		43.5%	13.8(±3.2%)	6.7		13.1	12.6	17.2	4.8×10^{24}	2.8	1.7, 7.9
L		First 12 hrs. after fatigue. T ≅ -95°C	6.50(± 6.2%)	4.5		6.35	6.05	8.17	5.57×10^{25}	4.6	[12] 1.4,14.1
	1	Second 12 hrs. after fatigue. T ≅ 25°C.	8.58(± 4.2%)	6.6		8.46	8.19	11.14	1.26×10^{25}	1.7	[13] 2.2,15.8
	[14] 2	T ≅ 25°C.	9.82(± 5.5%)	6.0		10.0	9.68	13.24	1.05×10^{25}	2.6	2.0,14.1
[15] T	1	Prefatigue	21.3(± .5%)	21.0	Yes	17.9	18.2	23.7	3.7×10^{24}	6.3	.40,3.5
		1.45	22.0(± .8%)	22.1		18.8	19.1	24.6	3.2×10^{24}	6.6	.38,3.5
		4.83	21.6(± .8%)	21.7		18.4	18.9	24.5	3.3×10^{24}	6.2	.63,5.3

				t_G (Å)		$\sqrt{\langle t^2 \rangle}$ (Å)	$\langle t^2 \rangle / \langle t \rangle$ (Å)	$\frac{\langle v^2 \rangle}{\langle v \rangle}$ (Å³)	$\langle D \rangle$ (Å)	Q	$\sqrt{I/I}$ (%)
T	2	Vertical	37.3(± .41%)	22.1		15.8	23.2	[16] 1.3×10^{6}	76.7	10.0	[17] .28,4.1
		Horizontal	39.0(± .63%)	31.7		24.2	34.8	2.4×10^{6}	87.0	3.7	.28,4.5
		45°	47.2(± .62%)	52.7		36.3	60.4	5.4×10^{6}	101.2	5.7	.21,3.7

1. The value in parenthesis is the standard deviation of the least squares fit to Guinier's approximation. Correlation coefficients for the Guinier least squares fit were all greater than .999. (The LS denotes values obtained from a least squares fit to Guinier and Porod approximations. SD denotes values obtained from the size distribution analysis.)

2. Average diameter derived from the size distribution.

3. Q is given in relative units. Although the statistical counting error involved in the sample (plus parasitic) and parasitic scattering patterns are very low, the determination of Q involves a larger uncertainty. The greatest uncertainty lies in the somewhat subjective choice of the angle at which to apply extrapolation, the range of h to be used for the least squares fit, and the form of the intensity in this range.

   Even though statistical counting error might only equal a few percent at the most, experience has shown that the uncertainty in Q can be as high as 20% since up to 50% of the intensity can come from the high angle region. As R_{PLS} and N_{TOT} (the GP zone density) depend directly on an accurate determination of Q, their relative errors would be similar in magnitude. No attempt was made to scale intensities between samples, so Q could vary from sample to sample due to filament, alignment, etc.

4. The statistical counting errors ($\sqrt{I}/I$), are given at the low angle interference maxima and high angle data points, respectively, where I is the number of accumulated counts.

   Data for this sample was collected to $h \cong .40\ \text{Å}^{-1}$.

5. Data collected to $h \sim .4\ \text{Å}^{-1}$; counting errors in parasitic scattering were .62% to 2.5%.

6. The vertical tilt data shown above differed from R_G calculated from a horizontal and 45° tilt by less than 10%.

7. A 45° sample tilt yielded $R_{GLS} = 16.6$ Å, $R_{PLS} = 13.1$, $Q = 3.2$.

8. A horizontal sample tilt yielded $R_{GLS} = 14.2$, $R_{PLS} = 10.3$, $Q = 5.3$.

9. Data collected to $h \sim .36\ \text{Å}^{-1}$. A parasitic scattering curve collected had counting errors ranging from .65% to 7.1%.

10. The as-quenched value of $Q = 5.1$.

11. This data corresponds to SAXS patterns collected after fatigue sets #7, 8, and 9.

12. Data collected at 178°K extended to $h \sim .53\ \text{Å}^{-1}$. A parasitic scattering pattern showed counting error ranging from ± .82% to ± 8.8%.

13. Data collected at 298°K extended to $h \sim .6\ \text{Å}^{-1}$.

14. A scattering pattern collected for this grain tilted horizontally yielded: $R_G \sim 9.7$, $Rp \sim 6.1$, $Q \cong 2.5$.

15. Data were collected out to $h \cong .36$ Å^{-1}.

16. The average diameter is estimated from the Guinier thickness, t_G, and the average volume $\langle V^2 \rangle / \langle V \rangle$. We assume that:

$$\langle D \rangle = \left(\frac{\langle V^2 \rangle}{\langle V \rangle \langle t \rangle} \right)^{\frac{1}{2}}$$

17. The data were collected to $h \cong .36$ Å^{-1}.

TABLE IV
Calculated Ostwald Ripening Kinetics

Sample ID	Composition (a/o)	$2R_{initial}$ (Å)	$2R_{final}$ (Å)	t (sec.)	$\Delta\varepsilon_{PL}^{max}$ (%)	$\sum_{t}^{7} \Delta\varepsilon_{PL}$ (%)	σ_{max} (MPa)	D(t) (m^2/sec)	N_V (atom fraction)
V	5.3	17.5	[1]24.8	1460	.16	3.5	224.1	3.4×10^{-11}	1.7×10^{-5}
S	5.3	19.5	[2]22.7	800	.16	6.8	184.8	2.7×10^{-11}	1.3×10^{-5}
P	3.5	9.1	[3]11.2	420	.05	6.5	76.5	7.8×10^{-12}	3.9×10^{-6}
P	3.5	11.2	[4]17.2	260	.11	36.5	113.1	7.1×10^{-11}	3.5×10^{-6}
L	3.5	2.0	8.2	[5]4.3×10^{4}	---	----	100.0	4.0×10^{-14}	1.6×10^{-2}
L	3.5	8.2	12.1	[6]3.6×10^{4}	---	----	----	1.7×10^{-13}	8.5×10^{-8}

[1] Final size of GP zones taken for grains #1 and #2. Constant volume fraction during growth (~ 5%).
[2] Particle growth during fatigue cycle set #2. Volume fraction increased from ~ 1% to ~ 3%.
[3] Particle growth during fatigue cycle set #8. Volume fraction increased from ~ 1.6% to 2.4%.
[4] Particle growth during fatigue cycle set #9. Constant volume fraction during growth (~ 2.4%).
[5] Particle growth from solid solution at $T \cong 178^{o}K$ in 12 hours during SAXS.
[6] Particle growth during initial 10 hours SAXS run at $298^{o}K$ Final size of GP zones taken from average of grains #1 and #2.
[7] The plastic strain given is that accumulated only in the time span of interest.

TABLE V

Experimental and Emperical Estimates of N_V

Sample ID	$\Sigma\Delta\epsilon_{PL}$ (%)	N_V(experimental) (atom fraction)	N_V(Seitz) (atom fraction)
V	3.5	1.7×10^{-5}	3.5×10^{-6}
S	6.8	1.3×10^{-5}	6.8×10^{-6}
P	6.5	3.9×10^{-6}	6.5×10^{-6}
P	36.5	3.5×10^{-5}	3.7×10^{-5}

FIGURE CAPTIONS

Fig. 1. Nominal dimensions of fatigue specimens, in millimeters.

Fig. 2. Schematic diagram of a fatigue hysterisis loop, with definition of terms.

Fig. 3. Sample V

a) Guinier plots, before and after failure.

b) G. P. zone size distributions.

Fig. 4. Guinier plots, sample T.

Fig. 5. Sample 8

a) Scattering patterns.

b) Zone size distributions.

Fig. 6. Sample P

a) Scattering patterns.

b) Zone size distributions.

Fig. 7. Sample L

a) Scattering patterns.

b) Zone size distributions.

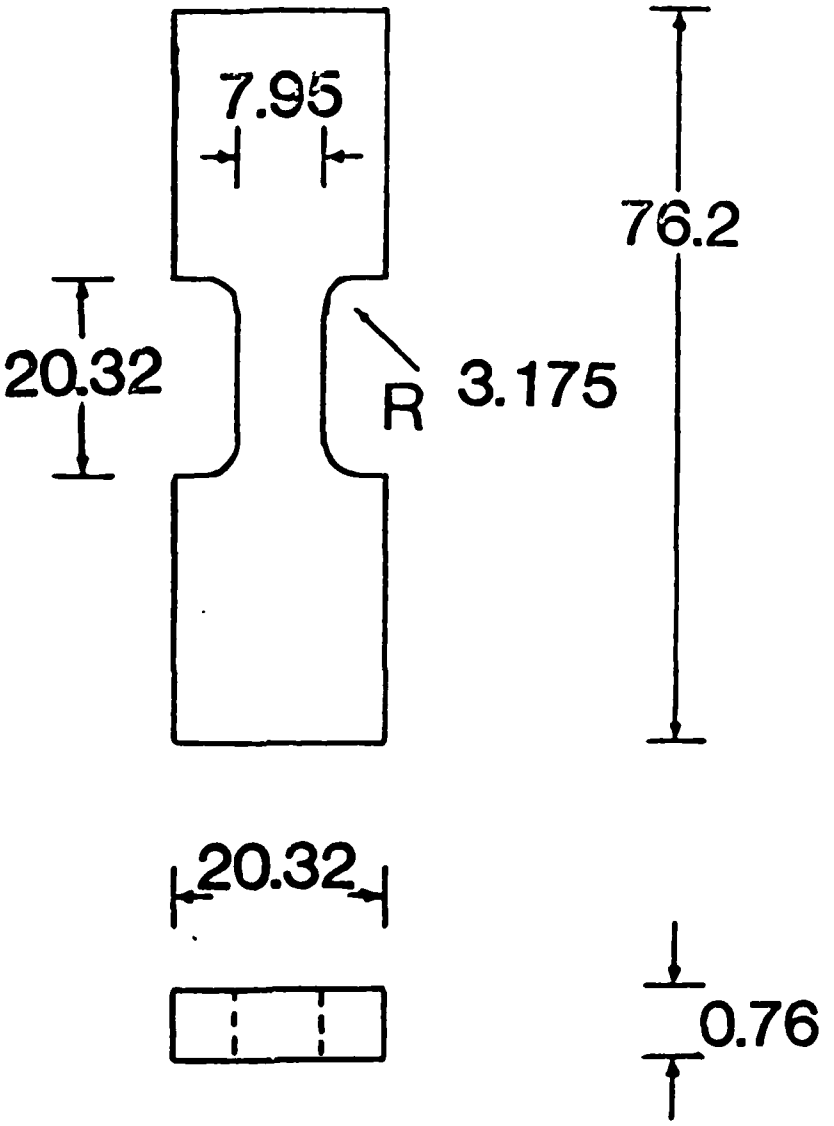

FIGURE 1

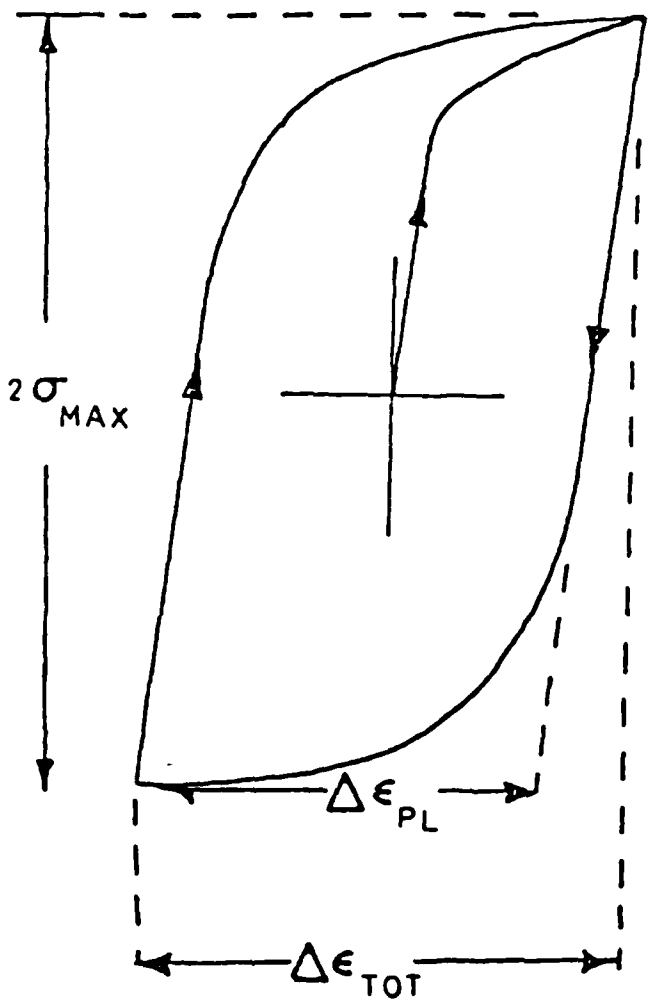

FIGURE 2

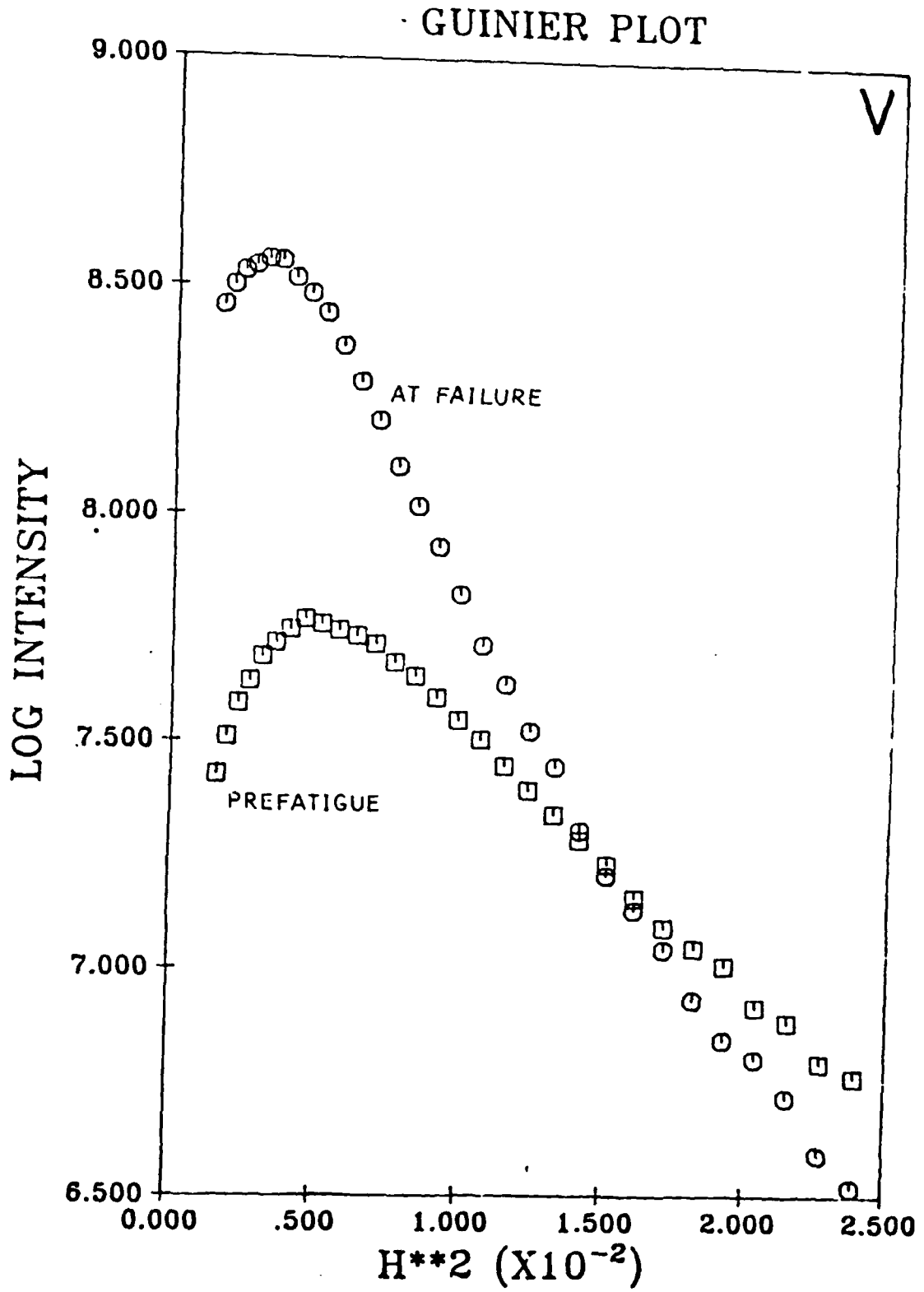

Fig. 3a R. G. Pahl, Jr. and J. B. Cohen

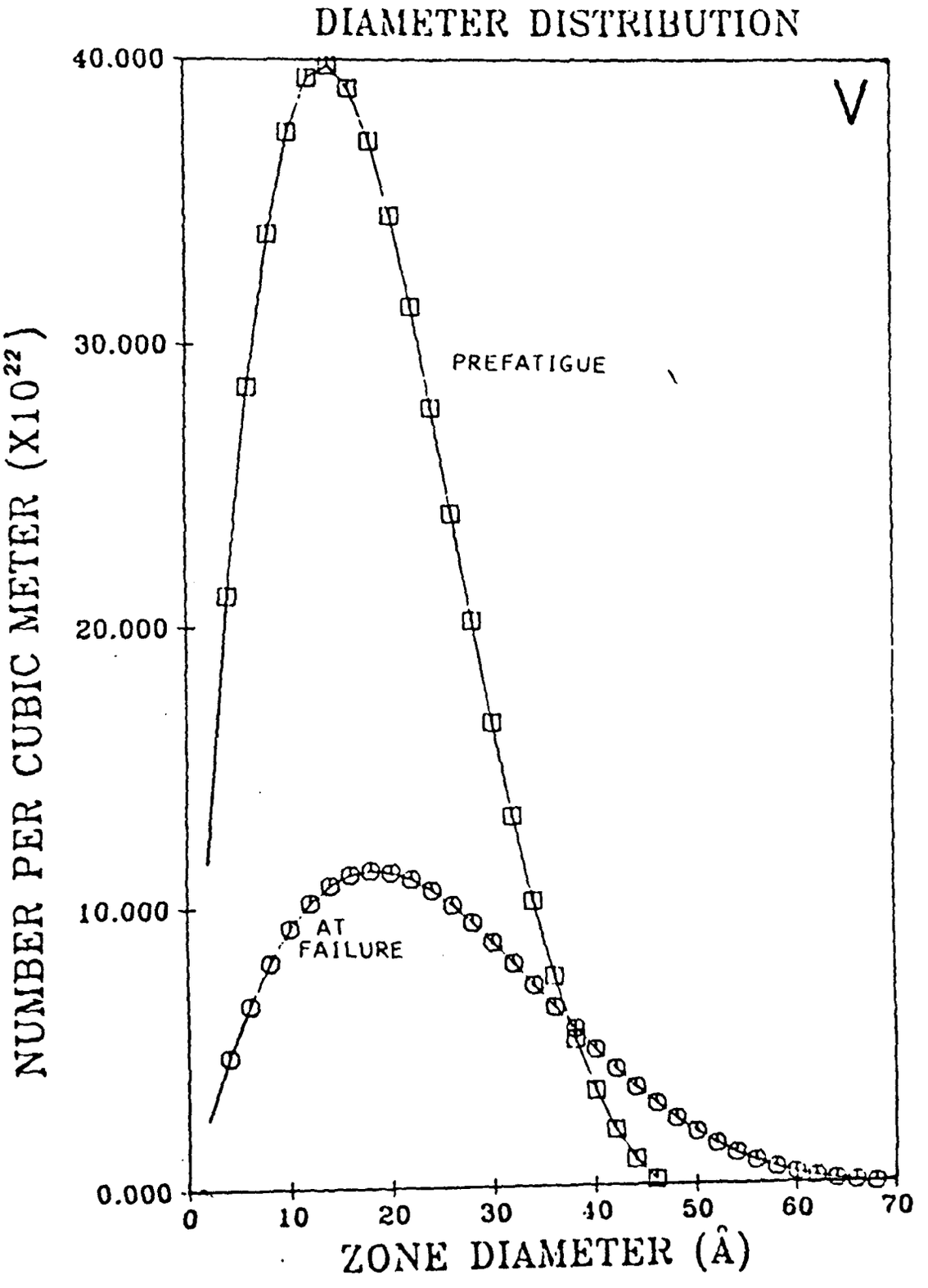

Fig. 3b R. G. Pahl, Jr. and J. B. Cohen

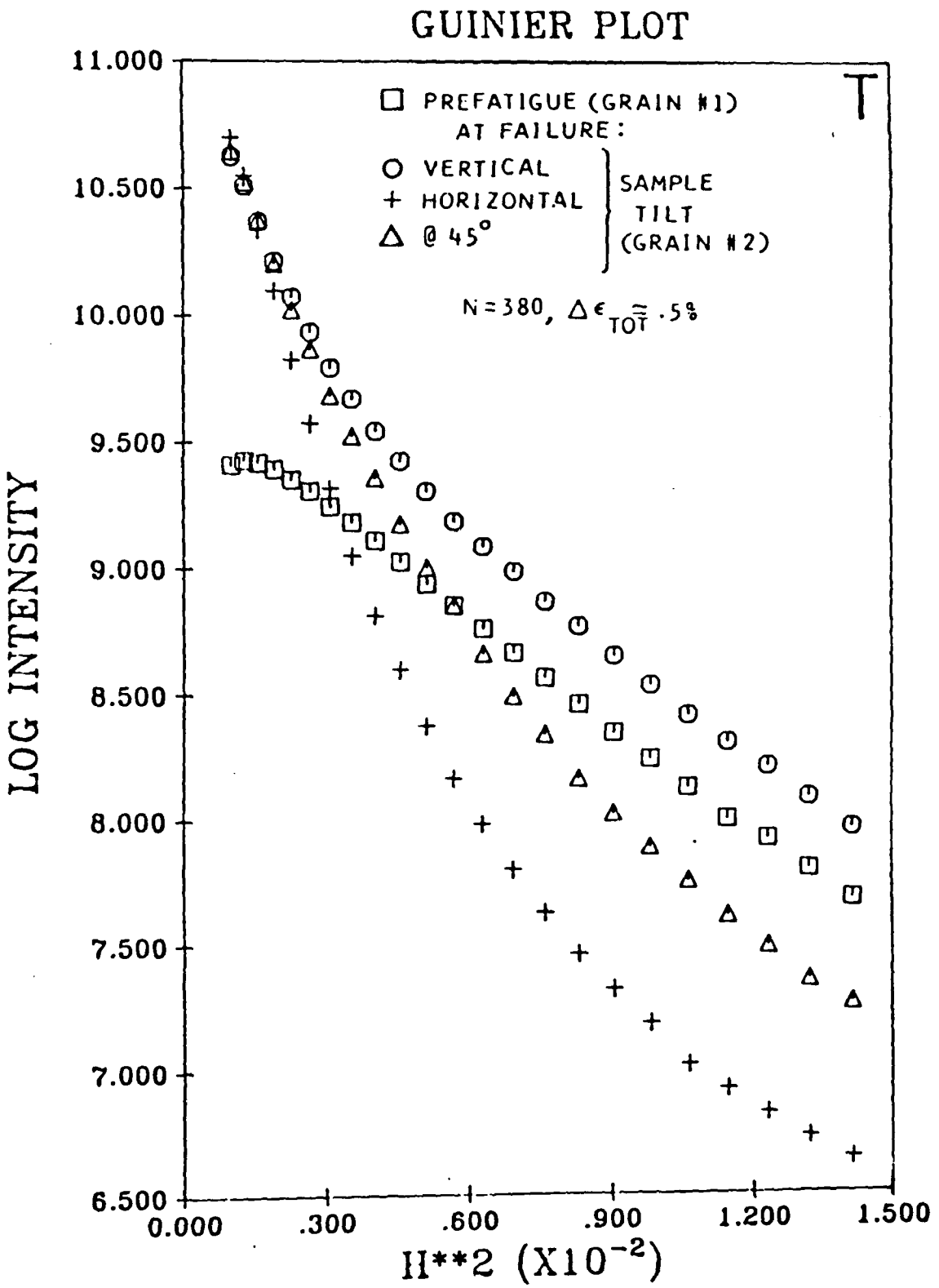

Fig. 4 R. G. Pahl, Jr. and J. B. Cohen

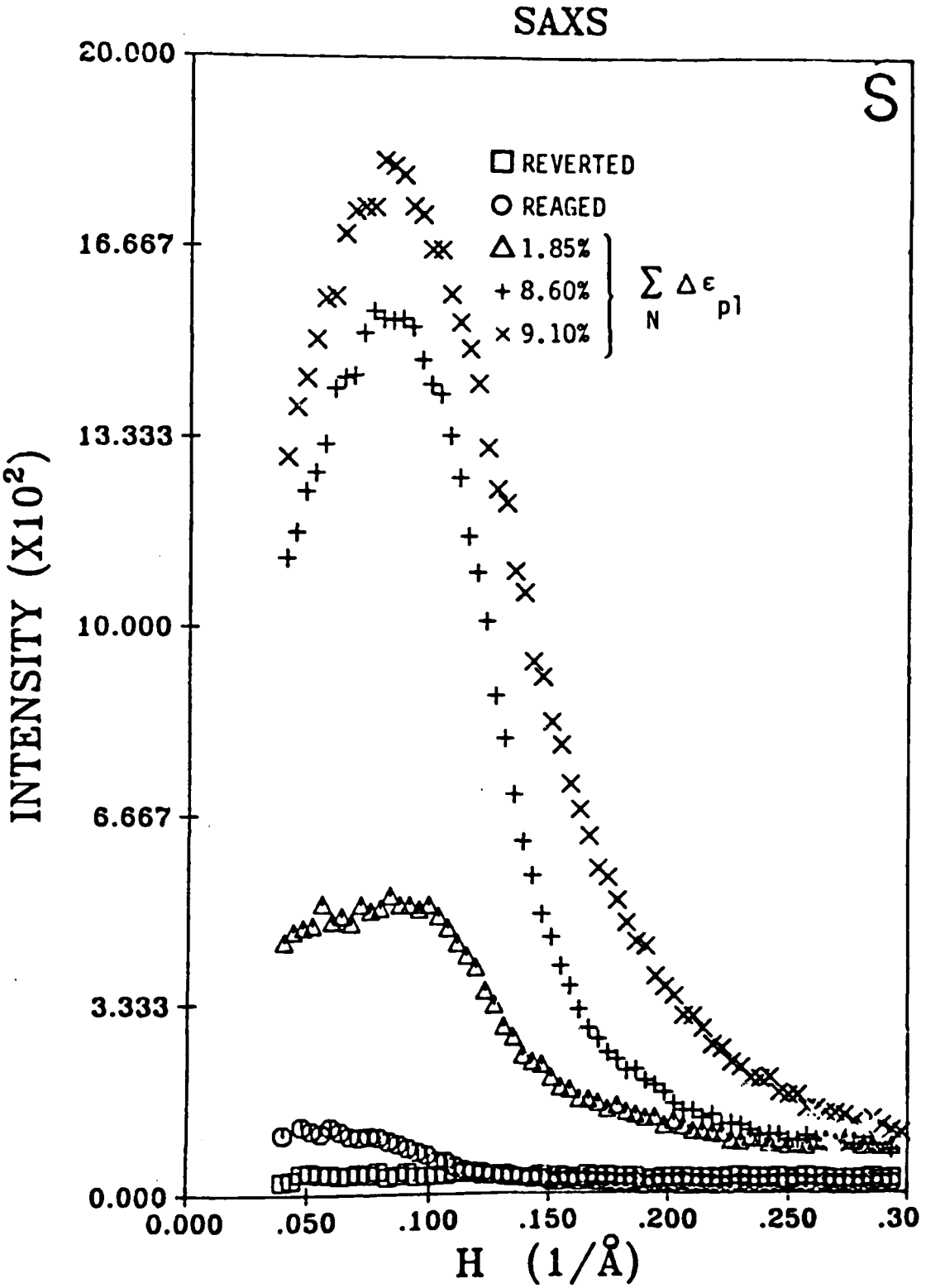

Fig. 5a R. G. Pahl, Jr. and J. B. Cohen

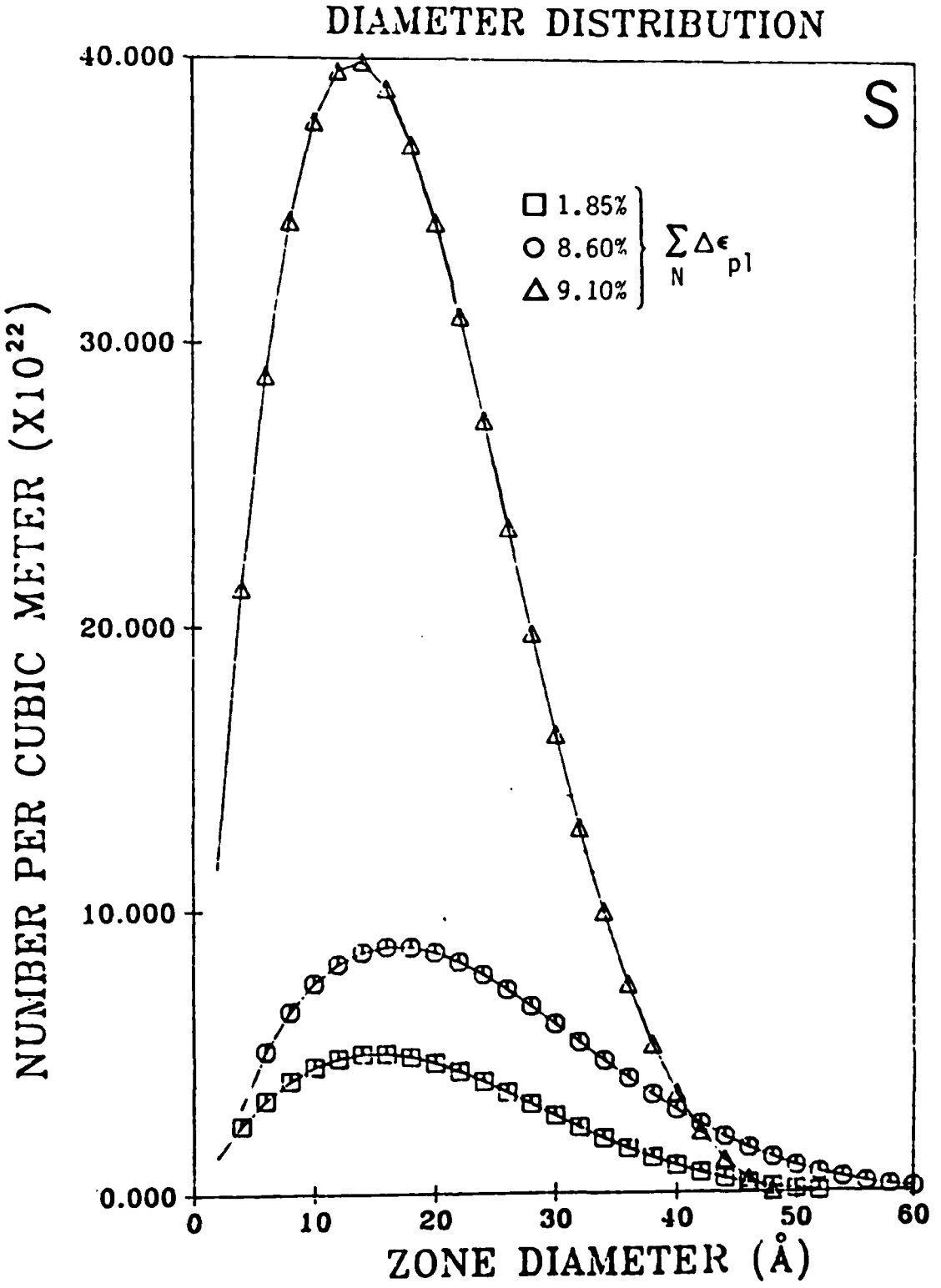

Fig. 5b R. G. Pahl, Jr. and J. B. Cohen

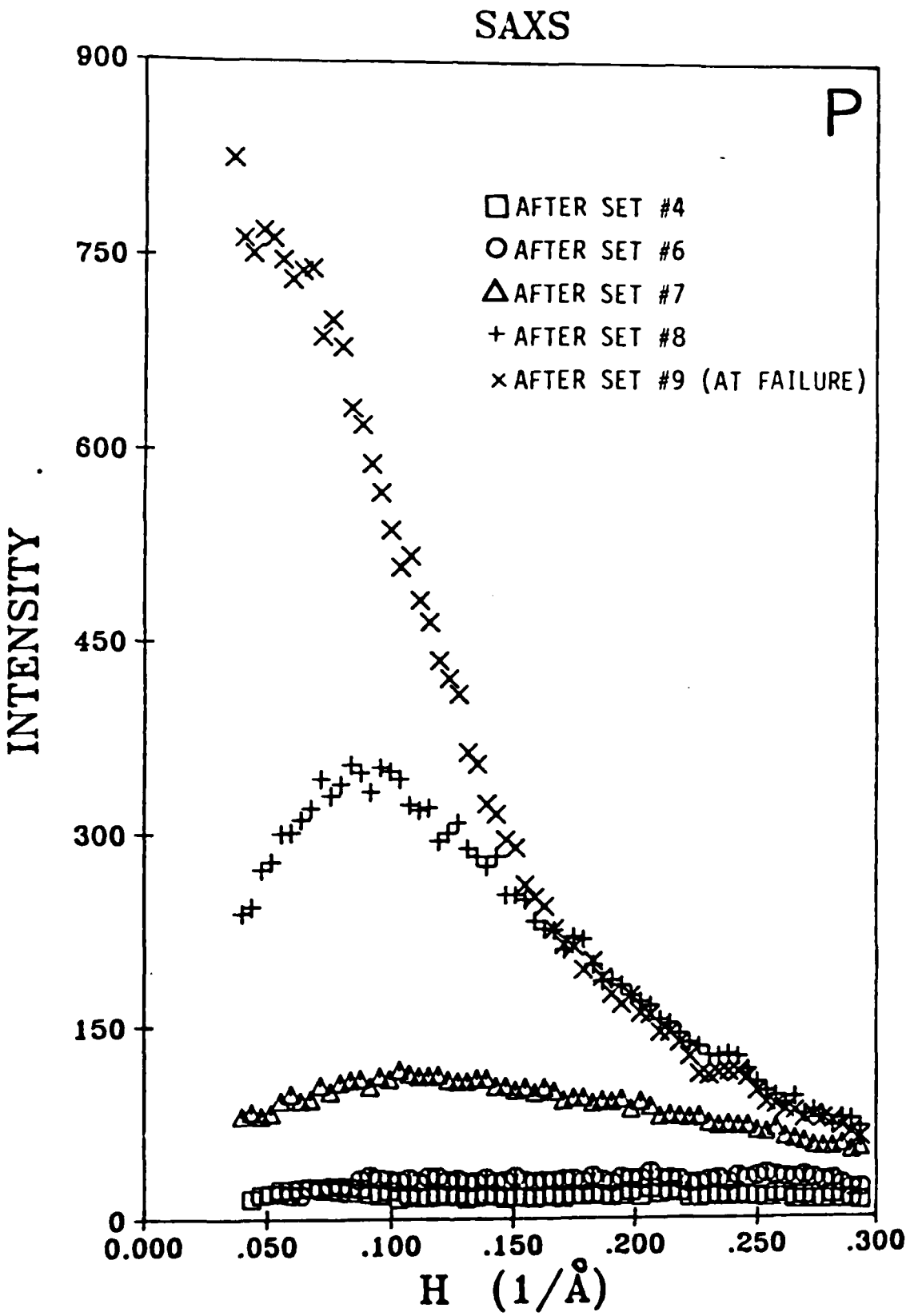

Fig. 6a R. G. Pahl, Jr. and J. B. Cohen

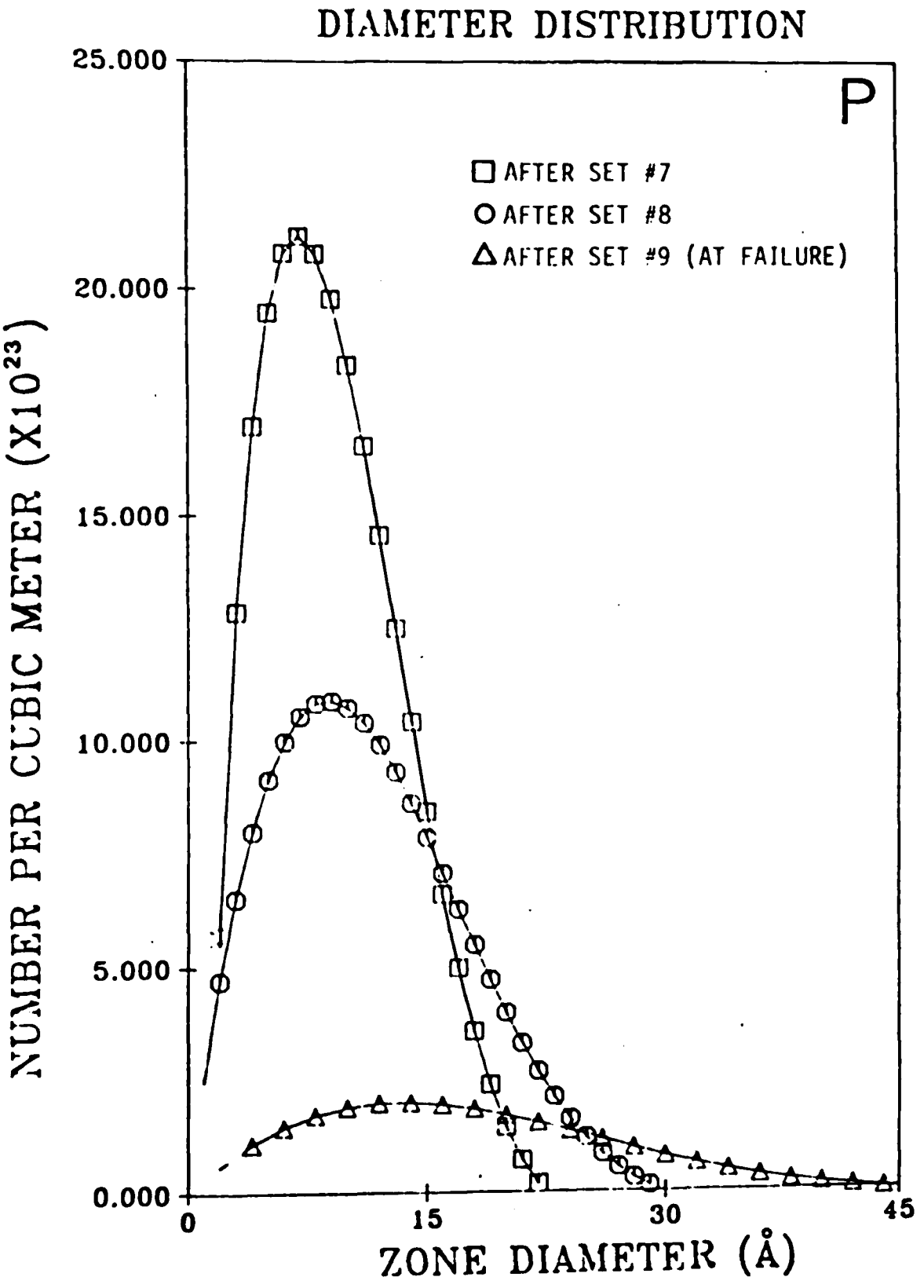

Fig. 6b R. G. Pahl, Jr. and J. B. Cohen

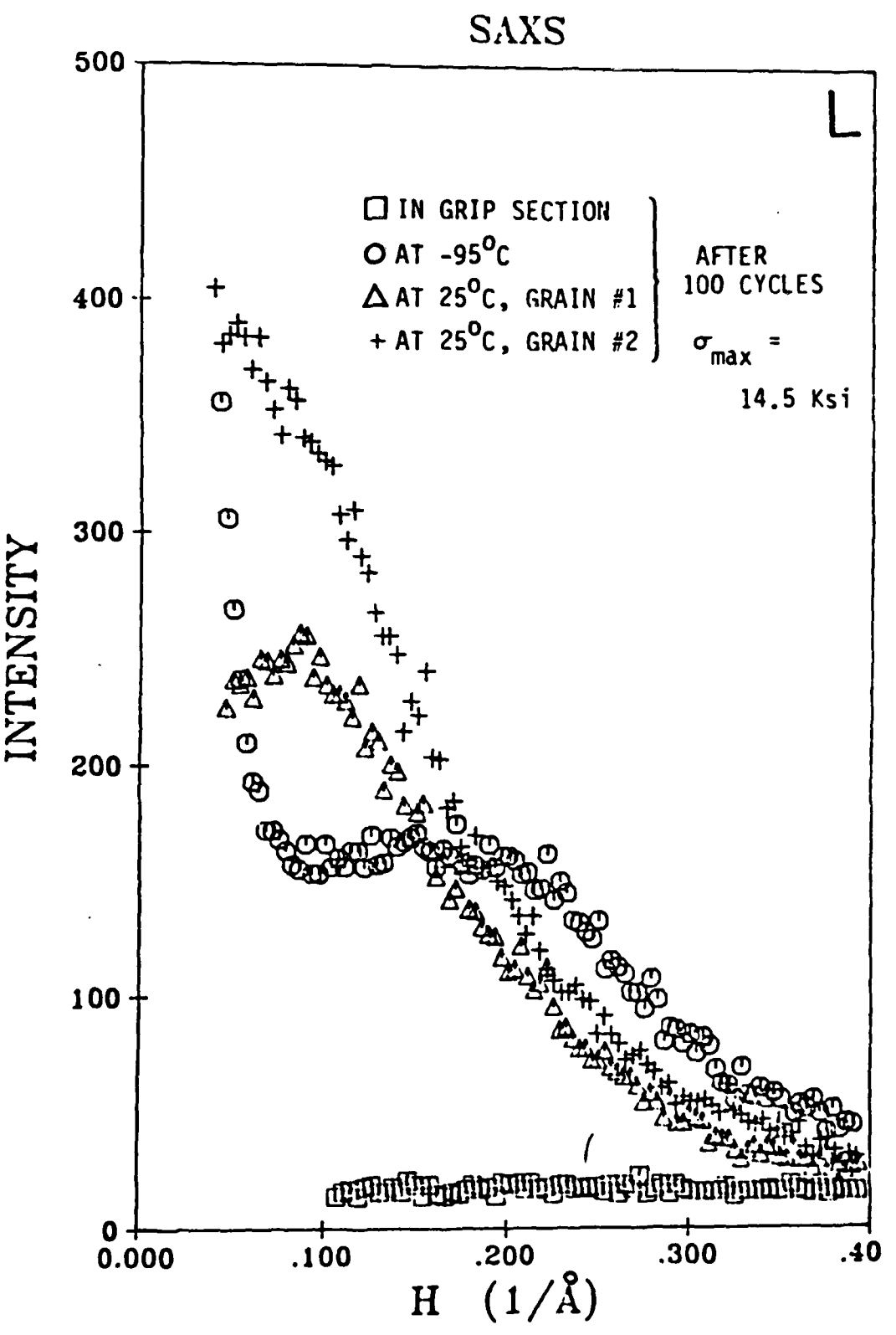

Fig. 7a R. G. Pahl, Jr. and J. B. Cohen

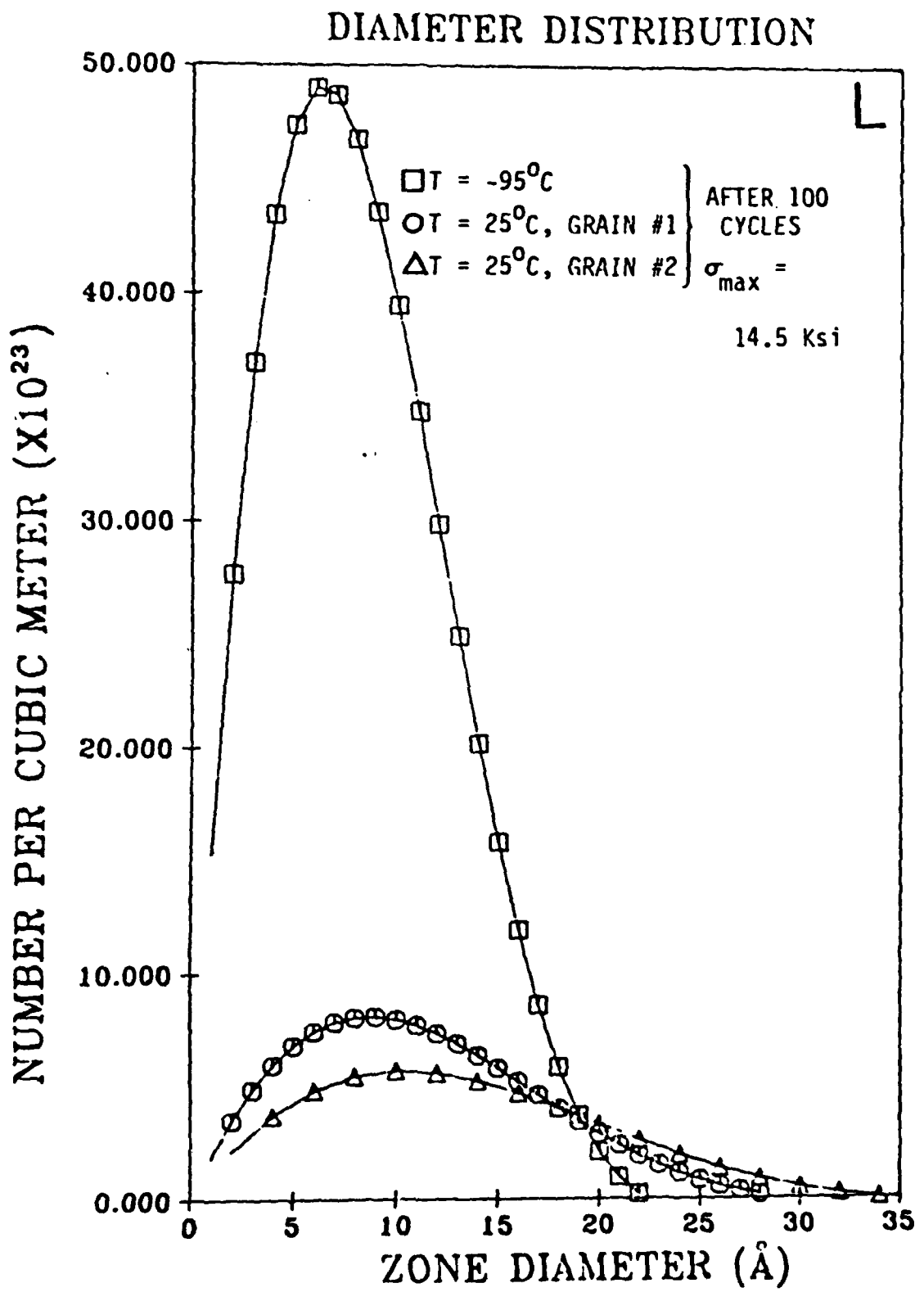

Fig. 7b R. G. Pahl, Jr. and J. B. Cohen

Security Classification

DOCUMENT CONTROL DATA - R & D

Security classification of title, body of abstract and indexing annotation must be entered when the overall report is classified)

1. ORIGINATING ACTIVITY (Corporate author)

J. B. Cohen
Northwestern University
Evanston, Illinois 60201

2a. REPORT SECURITY CLASSIFICATION

Unclassified

2b. GROUP

3. REPORT TITLE

EFFECTS OF FATIGUE ON THE G. P. ZONES IN Aℓ-Zn ALLOYS

4. DESCRIPTIVE NOTES (Type of report and inclusive dates)

Technical Report No. 13

5. AUTHOR(S) (First name, middle initial, last name)

R. G. Pahl, Jr. and J. B. Cohen

6. REPORT DATE	7a. TOTAL NO. OF PAGES	7b. NO. OF REFS
January 16, 1984		

8a. CONTRACT OR GRANT NO.	9a. ORIGINATOR'S REPORT NUMBER(S)
N00014-80-C-116	
b. PROJECT NO Mod. No. P00001	13
c.	9b. OTHER REPORT NO(S) (Any other numbers that may be assigned this report)
d.	

10. DISTRIBUTION STATEMENT

Distribution of this document is unlimited

11. SUPPLEMENTARY NOTES	12. SPONSORING MILITARY ACTIVITY
	Metallurgy Branch Office of Naval Research

13. ABSTRACT

Small-angle x-ray scattering has been applied to study the evolution and stability of G. P. zones in two Aℓ-Zn alloys during fatigue, to provide statistically sound information on this process. In a 5.3 at pct Zn alloy containing $\sim 10^{25}$ zones per m^3 with an average diameter of 18 Å, the normally sluggish coarsening was accelerated by fatigue at room temperature by 10^6 - 10^7. In the same alloy with larger zones (24 Å) there is no growth, except near a fatigue crack. Reverted samples aged rapidly during fatigue at room temperature, but in a reverted sample of Aℓ-3.5 at pct Zn tested at 77°K appreciable zone growth did not occur. Upon warming this sample (without any load) to room temperature, rapid clustering took place. These results imply a vacancy fraction produced during fatigue of ~~10^{-5}-10^{-6}~~, and this excess vacancy concentration appears to be the cause of zone growth during room temperature fatigue.

DD FORM 1 NOV 68 1473 (PAGE 1)

S/N 0101-807-6801

Security Classification

14 KEY WORDS	LINK A		LINK B		LINK C	
	ROLE	WT	ROLE	WT	ROLE	WT
fatigue, G. P. zones, G. P. zones and fatigue, fatigue softening						


DATE
ILME